Mineralogical Magazine, February 2017, Vol. 81(1), pp. 183–197

Nolzeite, $Na(Mn,\square)_2[Si_3(B,Si)O_9(OH)_2]\cdot 2H_2O$, a new pyroxenoid mineral from Mont Saint-Hilaire, Québec, Canada

Monika M. M. Haring* and Andrew M. McDonald

Department of Earth Sciences, Laurentian University, Sudbury, Ontario P3E 2C6, Canada

[*Received 9 November 2015; Accepted 31 January 2016; Associate Editor: Anthony Kampf*]

ABSTRACT

Nolzeite, $Na(Mn,\square)_2[Si_3(B,Si)O_9(OH)_2]\cdot 2H_2O$, is a new mineral found in altered sodalite syenite at the Poudrette quarry, La Vallée-du-Richelieu, Montérégie (formerly Rouville County), Québec, Canada. Crystals are colourless to pale green and are acicular with average dimensions of 5 μm × 8 μm × 55 μm. They occur as radiating to loose, randomly oriented groupings within vugs associated with aegirine, nepheline, sodalite, eudialyte-group minerals, analcime, natron, pyrrhotite, catapleiite, steedeite and the unidentified mineral, UK80. Nolzeite is non-pleochroic, biaxial, with n_{min} = 1.616(2) and n_{max} = 1.636(2) and has a positive elongation. The average of six chemical analyses gave the empirical formula: $Na_{1.04}(Mn_{1.69}\square_{0.24}Fe_{0.05}Ca_{0.02})_{\Sigma=2.00}(Si_{2.96}S_{0.04})_{\Sigma=3.00}(B_{0.70}Si_{0.30})_{\Sigma=1.00}O_9(OH)_2\cdot 2H_2O$ based on 13 anions. The Raman spectrum shows six distinct bands occurring at ~3600–3300 cm^{-1} and 1600–1500 cm^{-1} (O–H and H–O–H bending), 1300–1200 cm^{-1} (B–OH bending), 1030–800 cm^{-1} (Si–O–Si stretching) as well as 700–500 cm^{-1} and 400–50 cm^{-1} (Mn–O and Na–O bonding, respectively). The FTIR spectrum for nolzeite shows bands at ~2800–3600 cm^{-1} (O–H) stretching, a moderately sharp band at 1631 cm^{-1} (H–O–H) bending, strong, sharp bands at ~650–700 cm^{-1}, ~800–840 cm^{-1}, and ~900–1100 cm^{-1} (Si–O and B–O) bonds. Nolzeite is triclinic, crystallizing in space group $P\bar{1}$ with a = 6.894(1), b = 7.632(2), c = 11.017(2) Å, α = 108.39(3), β = 99.03, γ = 103.05(3)°, V = 519.27 $Å^3$, and Z = 2. The crystal structure was refined to R = 12.37% and wR^2 = 31.07% for 1361 reflections ($F_o > 4\sigma F_o$). It is based on chains of tetrahedra with a periodicity of three (i.e. a *dreier* chain) consisting of three symmetrically independent SiO_4 tetrahedra forming *C*-shaped clusters closed by $BO_2(OH)_2$ tetrahedra, producing single loop-branched *dreier* borosilicate chains. The chains are linked through shared corners to double chains of edge-sharing $MnO_5(OH)$ octahedra. Nolzeite is a chain silicate closely related to steedeite and members of the sérandite–pectolite series. Paragenetically, nolzeite is late-stage, probably forming under alkaline conditions and over a narrow range of low pressures and temperatures.

Keywords: new mineral species, nolzeite, Mont Saint-Hilaire, crystal structure, borosilicate, sérandite–pectolite, loop-branched dreier chain, Fourier transform infrared spectrum, Raman spectrum.

Introduction

Nolzeite, ideally $Na(Mn,\square)_2Si_3(B,Si)O_9(OH)_2\cdot 2H_2O$, is a new borosilicate from Mont Saint-Hilaire, Québec, Canada, one of the world's most prolific localities for new minerals (Chao *et al*., 1990). It was investigated as part of a broader examination of borosilicate minerals found at this locality, a list of which currently numbers 12. The mineral occurs as fine acicular crystals with a small size that initially inhibited determination of its structure via standard single-crystal diffractometers employing scintillation detectors. Determination and refinement of the crystal structure were critical not only to confirming the presence of both H_2O and (OH) in the mineral but also in recognizing that the mineral contains essential B_2O_3. In this contribution we present a complete crystal-chemical characterization of nolzeite, elucidate the relationship of this mineral to members of the

* E-mail: mharing53@gmail.com
https://doi.org/10.1180/minmag.2016.080.089

sérandite–pectolite series and provide insights into the conditions that led to its formation. Nolzeite is named for Dr. Gert Nolze (b. 1960), a crystallographer at the Federal Institute for Materials Research and Testing (BAM), Berlin, Germany. Dr. Nolze, in conjunction with Dr. Werner Kraus, developed *Powdercell* (Kraus and Nolze, 1996; currently in ver. 2.4), a program that has been used extensively in the calculation of powder X-ray diffraction patterns of minerals. Dr. Nolze is an expert in the field of electron microbeam techniques, in particular, electron back-scatter diffraction (EBSD) and he has applied his knowledge to the study of minerals in meteorites (Nolze *et al*., 2005). Both the mineral and mineral name have been approved by the International Mineralogical Association, Commission on New Minerals and Mineral Names (IMA 2014–086). The holotype material is housed in the collections of the Canadian Museum of Nature (Gatineau, Quebec, Canada), catalogue number CMNMC 86851.

Occurrence

Nolzeite was discovered by Col. Quintin Wight in August 1987 and was provisionally designated UK78. The mineral was found initially in ~1 cm diameter vugs in a loose boulder (~1 m × 1 m) of sodalite syenite at the Poudrette quarry, La Vallée-du-Richelieu, Montérégie (formerly Rouville County), Québec, Canada (45°33′8″N, 73°9′3″W). The loose boulder was found in the south-east portion of the quarry, in proximity to a large number of so-called sodalite syenite xenoliths (tawites) in nepheline syenite (McDonald and Chao, 2010; McDonald and Chao, 2005). The boulder containing nolzeite was first noted because of the unusually high concentration of relatively thick, euhedral plates of pyrrhotite contained within it. When the boulder was broken up, numerous, centimetre-sized vugs filled with clear, crystalline natron ($Na_2CO_3 \cdot 10H_2O$) or natrite (Na_2CO_3) were exposed. These minerals subsequently decrepitated to thermonatrite ($Na_2CO_3 \cdot H_2O$) and related minerals. The sample containing nolzeite consists predominantly of microcline, analcime, nepheline along with aegirine, and pyrrhotite (Table 1). The pyrrhotite associated with nolzeite is magnetic, suggesting that it is the monoclinic 4*C* polytype. The rest of the sample is dominated by sodalite, a eudialyte-group mineral, sérandite, and thermonatrite (Table 1). Interestingly, some crystals of sodalite are found to atypically retain a pronounced violet colour even after prolonged exposure (i.e. several years) to light. The sérandite is highly unusual for the locality, ranging in colour from dark to pale green and brown to light brown unlike the much more typical pink to orange colouration that characterizes the mineral in other environments at Mont Saint-Hilaire. This green to brown colouration is attributed to trace amounts of Fe in the sérandite. It may also be noteworthy that sérandite, steedeite [$NaMn_2Si_3BO_9(OH)_2$; Haring and McDonald (2014)] and nolzeite, although occurring in the same samples, have not been specifically found together in the same vug. These minerals are all late-stage phases, having a strong crystal-chemical similarity, implying they all formed under similar geochemical conditions.

Physical and optical properties

Crystals of nolzeite are euhedral, acicular and elongate along [001], occurring in slightly radiating to loose, randomly oriented groupings ('nests'; Fig. 1). They exhibit the forms pinacoid {100}, pinacoid {010} and pinacoid {001}. Crystals have average dimensions 5 μm × 8 μm × 55 μm and average length-to-width ratios of ~69–110. They are pale green to colourless with a white streak and a vitreous lustre. Nolzeite shows no fluorescence under shortwave, mediumwave, or longwave UV radiation unlike the closely related species steedeite. This feature may thus be useful in distinguishing between the two minerals. Due to the small size of the crystals, a Mohs hardness for nolzeite could not be measured. A density of 2.79 g/cm^3 was calculated using the empirical chemical formula and unit-cell parameters derived from the crystal-structure analysis.

Nolzeite is assumed to be a biaxial, based on its crystal system. A complete set of optical data could not be collected due to the small crystal size and highly acicular habit of the mineral. It exhibits a positive elongation and refractive indices of n_{min} = 1.616(2) and n_{max} = 1.636(2) as measured with a Na-vapour lamp (λ = 589 nm). These refractive indices are lower than those of steedeite (n_{min} = 1.636 (2) and n_{max} = 1.656(2)) (Haring and McDonald, 2014) and sérandite–pectolite (n_{min} = 1.674(2) and n_{max} = 1.710(2)) possibly due to the more hydrous chemistry of nolzeite compared to steedeite and sérandite–pectolite. No pleochroism was observed. The Gladstone-Dale relation (Mandarino, 1981) gives a compatibility index $1 - (K_P/K_C) = 0.020$ (excellent) using the empirical formula and unit-cell

TABLE 1. Description and modal abundances of minerals occurring with nolzeite.

Mineral	Modal abundance	Description
Microcline $(KAlSi_3O_8)$	~68%	Aggregates of anhedral light grey crystals with a massive habit and greasy lustre.
Analcime $Na_2(Al_2Si_4O_{12})\cdot 2H_2O$	~10%	Anhedral to subhedral translucent to transparent crystals with a vitreous lustre.
Nepheline $(Na,K)AlSiO_4$	~7%	Anhedral, greenish-grey crystals with a greasy lustre.
Aegirine $NaFe^{3+}Si_2O_6$	~5%	Dark green, prismatic, euhedral crystals ranging in size from ~0.1 to 0.7 mm long and dominated by the form prism {110}.
Pyrrhotite $Fe_{1-x}S$	~5%	Pseudohexagonal crystals, ~4 mm in diameter, displaying the forms pinacoid {001}, pinacoid {100}, prism {100}, and prism {*h*0*l*}.
Sodalite $Na_8(Al_6Si_6O_{24})Cl_2$	~2%	Anhedral, transparent crystals with a pale blue to violet colour and a strong fluoresence under shortwave, mediumwave, and longwave radiation.
Eudialyte-group mineral $Na_{15}Ca_6(Fe^{2+}, Mn^{2+})_3Zr_3[Si_{25}O_{73}](O,OH,H_2O)_3(OH,Cl)_2$	~1%	Euhedral, translucent to transparent crystals with a dark brown to orange colour.
Sérandite $Na(Mn^{2+},Ca)_2Si_3O_8(OH)$	~1%	Radiating spheres composed of prismatic crystals with flattened terminations (pinacoid {001}). These crystals range in colour from dark to pale green and brown to light brown.
Thermonatrite $Na_2CO_3\cdot H_2O$	~1%	White anhedral to subhedral, translucent crystals.
Catapleiite $(Na,Ca,\square)_2ZrSi_3O_9\cdot 2H_2O$	trace	Clear, colourless, pseudohexagonal plates overgrowing sérandite.
Steedeite	trace	Clusters of radiating to randomly oriented, acicular, white to light pink crystals with dimensions similar to those of nolzeite.
UK80	trace	Flat clusters of radiating, brown crystals with dimensions similar to those of nolzeite.

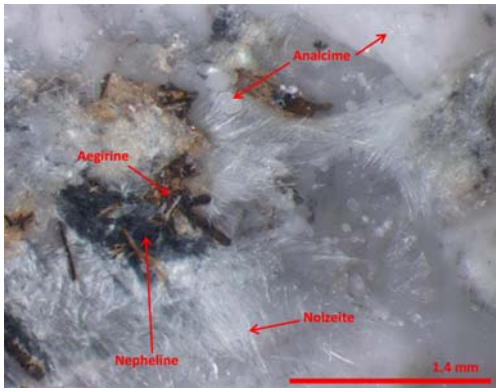

FIG. 1. Loose aggregates of nolzeite with nepheline, aegirine and analcime.

parameters derived from the crystal structure analysis.

Chemical composition

Chemical analyses of nolzeite were collected using a JEOL JSM 6400 scanning electron microscope equipped with an energy-dispersive spectrometer and operating conditions of: voltage = 20 kV, a beam current of ~1 nA and a beam width of ~1 μm (Central Analytical Facility, Laurentian University). Energy-dispersive data were collected using the following standards: albite (Na*K*α), diopside (Ca*K*α, Si*K*α), tephroite (Mn*K*α), and chalcopyrite (Fe*K*α, S*K*α). Chemical analyses (n = 6) of four crystals gave an average (range, standard deviation) of: Na_2O 7.34 (6.30–8.10, 0.66), CaO 0.29 (0.21–0.35, 0.05), MnO 27.29 (25.99–28.52,

0.97), FeO 0.83 (0.76–0.93, 0.08), SiO_2 44.17 (43.30–45.35, 0.79), SO_3 0.67 (0.35–1.02, 0.30), B_2O_3 (calc.) 5.45, and H_2O (calc.) 12.16, total 98.20 wt.%. The empirical formula based on 13 anions is: $Na_{1.04}(Mn_{1.69}\square_{0.24}Fe_{0.05}Ca_{0.02})_{\Sigma=2.00}(Si_{2.96}S_{0.04})_{\Sigma=3.00}(B_{0.70}Si_{0.30})_{\Sigma=1.00}O_9(OH)_2\cdot 2H_2O$ or ideally $Na(Mn,\square)_2[Si_3(B,Si)O_9(OH)_2]\cdot 2H_2O$. The ideal formula requires: Na_2O 7.24, MnO 28.16, SiO_2 46.30, B_2O_3 5.69, and H_2O 12.62 wt.%, total 100.00 wt.%, assuming that the *Mn* sites are 85% occupied and the *B* site is fully occupied with a substitution of 30% Si. Amounts of B, OH, and H_2O were calculated based on electroneutrality considerations and their presence was confirmed through a combination of crystal-structure and infrared analyses (see below), respectively. The presence of B was further confirmed through qualitative analyses made by scanning electron microscopy (SEM) with energy dispersive spectroscopy (EDS) using an operating voltage of 5 kV, a beam current of ~1 nA, a beam diameter of ~1 μm, a 15 s count time (longer count times led to sample degradation) and a light-element detector. The samples were Au-coated so as to mitigate problems associated with the near-overlap of C and B in EDS spectra. Results show that the EDS spectra of nolzeite and a tourmaline-supergroup mineral both contain peaks at ~0.17 keV (Fig. 2) which can be attributed to B (ideally, B*K*α = 0.183 eV), confirming the presence of B in both minerals. Nolzeite does not effervesce in 10% HCl at room temperature.

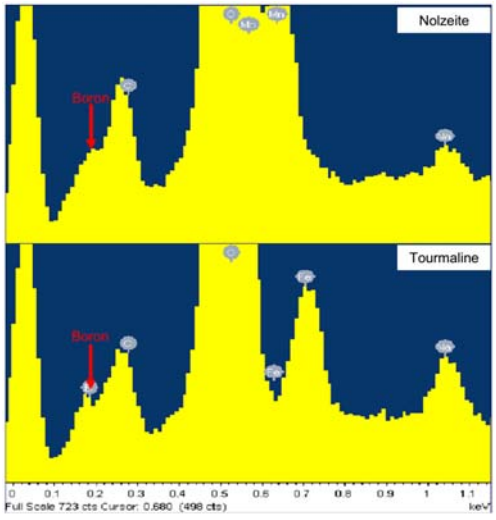

FIG. 2. Overlay of the EDS spectra for nolzeite and a tourmaline-supergroup mineral showing distinctive peaks with similar intensities, attributable to B*K*α. The presence of C is attributed to contamination.

Raman spectroscopy

A Raman spectrum of nolzeite, based on an average of three 20 s acquisition cycles over a range of 50 to 4000 cm^{-1}, was collected using a Horiba Jobin Yvon XPLORA Raman spectrometer interfaced with an Olympus BX41 microscope (Central Analytical Facility, Laurentian University). An excitation radiation of λ = 638 nm was used along with a 600 lines/mm grating and 100 × magnification (producing a beam of diameter of ~2 μm). The excitation radiation of λ = 638 nm was chosen to minimize fluorescence peaks in the region of ~2000 to 2800 cm^{-1} that were observed when the mineral was analysed using the more typically employed radiation of λ = 532 nm. Calibration was made using the 521 cm^{-1} line of a silicon wafer. Six distinct groups of bands occur in the Raman spectrum of nolzeite at ~3600–3300 cm^{-1}, 1600–1500 cm^{-1}, 1300–1200 cm^{-1}, 1030–800 cm^{-1}, 700–500 cm^{-1} and 400–50 cm^{-1} (Fig. 3). The first of these bands at ~3600–3300 cm^{-1} consists of two broad, low-intensity peaks that are attributed to O–H stretching (Table 2) (Williams, 1995). The next band at 1600–1500 cm^{-1} contains a single sharp, moderate intensity peak at 1586 cm^{-1} attributed to H–O–H bending. A single moderately sharp, low-intensity peak occurs in the band at 1300–1200 cm^{-1} at 1290 cm^{-1}. A similar peak can also be found in the Raman spectrum of steedeite at 1368 cm^{-1} (Haring and McDonald, 2014). The Raman spectrum of steedeite (Table 2) was calculated using the computer programs *Gaussian* (Frisch *et al*., 2013) and *Vibratz* (Dowty, 2009) so as to confirm band assignments for both nolzeite and steedeite. Given the chemical and structural similarities between steedeite and nolzeite, it is likely that the peak at 1290 cm^{-1} in the spectrum of nolzeite is also the result of B–OH bonding. The reason for the shift in the B–OH peak in nolzeite relative to steedeite is unknown. An increase in the Si↔B substitution is expected to cause the B–OH peak to shift higher wavenumbers in the Raman spectrum of nolzeite compared to that of steedeite. Instead the opposite is observed where the B–OH peak in the spectrum nolzeite is observed at lower wavenumbers than the corresponding peak in the spectrum of steedeite. The Raman band at 1030–800 cm^{-1} contains two sharp, low intensity peaks at

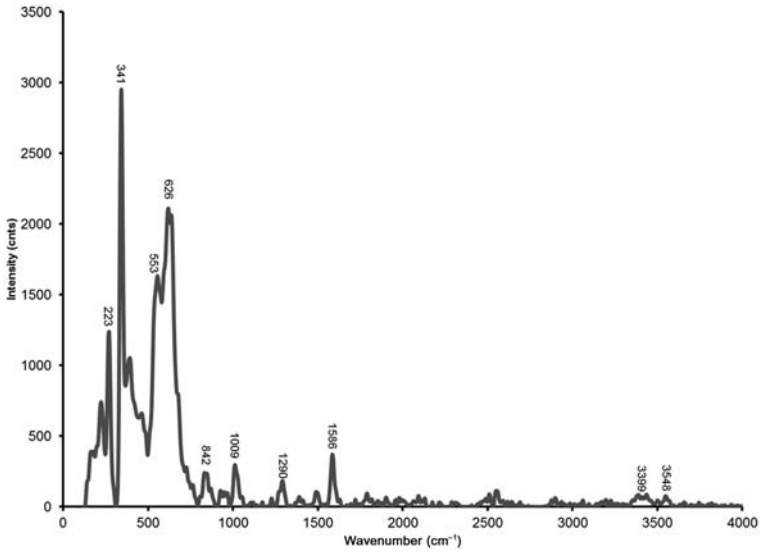

FIG. 3. Raman spectrum for nolzeite.

1009 and 842 cm^{-1} attributed to asymmetric $Si–O_{nbr}$/B–O stretching and symmetric Si–O stretching respectively (Williams, 1995). Similar peaks occur in steedeite at 874 and 1000 cm^{-1} but these are sharper with higher intensities compared to those in nolzeite. Furthermore, the peak at 842 cm^{-1} in nolzeite is at a lower wavenumber compared to the equivalent peak in steedeite, this being attributed to the slightly longer and lower energy Si–O. The band at 700–500 cm^{-1} contains two sharp, high intensity peaks at 626 and 553 cm^{-1}. These peaks are attributed to a combination of Si–O–Si bending and Mn–O bonding (Williams, 1995). Finally the band at 400–50 cm^{-1} contains five sharp, low to high intensity peaks at 390, 341, 268, 223 and 167 cm^{-1} attributed to Mn–O as well as Na–O bonding. Steedeite and nolzeite may be distinguished based on their Raman spectra. Unlike the Raman spectrum of nolzeite, the Raman spectrum of steedeite contains no peaks in the region of 1500–1600 cm^{-1} (H–O–H bending). Furthermore, the peaks in the spectrum of nolzeite tend to occur at lower wavenumbers than those of steedeite due to the longer Si–O bonds in nolzeite (see discussion above).

Infrared spectroscopy

An infrared (FTIR) spectrum (Fig. 4) was collected over a range of 600 to 4000 cm^{-1} using a Bruker Alpha spectrometer (Department of Chemistry and Biochemistry, Laurentian University) equipped with a KBr beam splitter and a DTGS detector. The spectrum, obtained by averaging 128 scans with a resolution of 4 cm^{-1}, reveals five distinct bands at ~650–700 cm^{-1}, 800–840 cm^{-1}, 900–1100 cm^{-1}, 1631 cm^{-1}, ~2800–3600 cm^{-1}. The 800–840 cm^{-1} are associated with symmetric Si–O bending, and the bands at 900–1100 cm^{-1} are associated with asymmetric Si–O bending or possibly B–O bending (Frost *et al*., 2007; Williams, 1995). The remaining bands at 1631 cm^{-1} and ~2800–3600 cm^{-1} are associated with H–O–H and O–H bending, respectively (Williams, 1995). Peaks associated with Na–O bonds tend to occur below 600 cm^{-1} and were thus not detected. The FTIR and Raman spectra for nolzeite both show a peak in the region of 600 to 700 cm^{-1} but that in the FTIR spectrum occurs at a higher wavenumber (697 cm^{-1}) than the equivalent in the Raman spectrum (626 cm^{-1}). In addition, both spectra show peaks in the region of 800 to 1100 cm^{-1} however, more peaks with higher intensities occur in the 800 to 1100 cm^{-1} region of the FTIR spectrum. This could be due to the fact that crystals of nolzeite were powdered to make a KBr pellet for FTIR analysis, whereas Raman analysis was conducted on single crystals. The powdering of nolzeite during the preparation of KBr pellets would have minimized preferred-orientation effects. Finally the FTIR spectrum,

TABLE 2. Absorption bands (cm^{-1}) and band assignments for the Raman spectra of nolzeite and steedeite.

Nolzeite	Steedeite*	Steedeite, calculated	Assignments
3548	–	–	O–H Stretching
–	3443	3450	O–H Stretching
3399	–	–	O–H Stretching
–	3317	–	O–H Stretching
–	1700	–	Unassigned
1586	–	–	H–O–H bending
–	1368	–	B–OH bonds
–	–	1342	B–OH bonds
1290	–	–	B–OH bonds
–	1030	1021	Asymmetric Si–O_{nbr}/B–O stretching
1009	1000	1006	Asymmetric Si–O_{nbr}/B–O stretching
–	874	876	Symmetric Si–O_{br} stretching
842	–	–	Symmetric Si–O_{br} stretching
–	–	852	Symmetric Si–O_{br} stretching
–	826	–	Symmetric Si–O_{br} stretching
–	696	690	Si–O–Si Bending
626	636	624	Si–O–Si Bending/Mn–O
553	–	–	Si–O–Si Bending/Mn–O
–	–	451	Si–O–Si Bending/Mn–O
–	431	–	Mn–O
390	–	–	Mn–O
341	–	–	Mn–O
–	–	366	Mn–O
–	330	–	Mn–O
–	–	289	Mn–O
268	264	–	Mn–O/Na–O
223	–	–	Na–O
–	197	–	Na–O
–	–	156	Na–O
167	–	–	Na–O

*Haring and McDonald (2014).

unlike the Raman spectrum, shows distinct bands in the regions of ~1600–1700 cm^{-1} and ~2800–3600 cm^{-1} attributed to H–O–H and O–H bending. The bands attributed to O–H and H–O–H are weak to non-existent in the Raman spectrum, possibly owing to the low polarizability of H–O bonds.

X-ray crystallography and crystal structure determination

Powder X-ray diffraction data were collected using a 114.6 mm diameter Gandolfi camera, 0.3 mm collimator, and Fe-filtered Co$K\alpha$ radiation (λ = 1.7902 Å). Intensities were determined using a scanned image of the powder pattern and normalized to the measured intensity of d = 10.113 Å (I = 100). A calculated X-ray pattern, determined using the results from the crystal-structure analysis and the program *PowderCell* (Kraus and Nolze, 1996), is in good agreement with the observed pattern (Table 4).

X-ray intensity data were collected on a Bruker D8 three-circle diffractometer (Department of Geological Sciences, University of Manitoba) equipped with a rotating-anode generator, multilayer optics incident beam path and an APEX-II CCD detector. X-ray diffraction data (9610 reflections) were collected to 60°2θ using 20 s per 0.3° frame with a crystal-to-detector distance of 5 cm. The unit-cell parameters were obtained by least-squares refinement of 2706 reflections ($I > 10\sigma I$), and are given in Table 3. Empirical absorption corrections (*SADABS*; Sheldrick, 1998) were

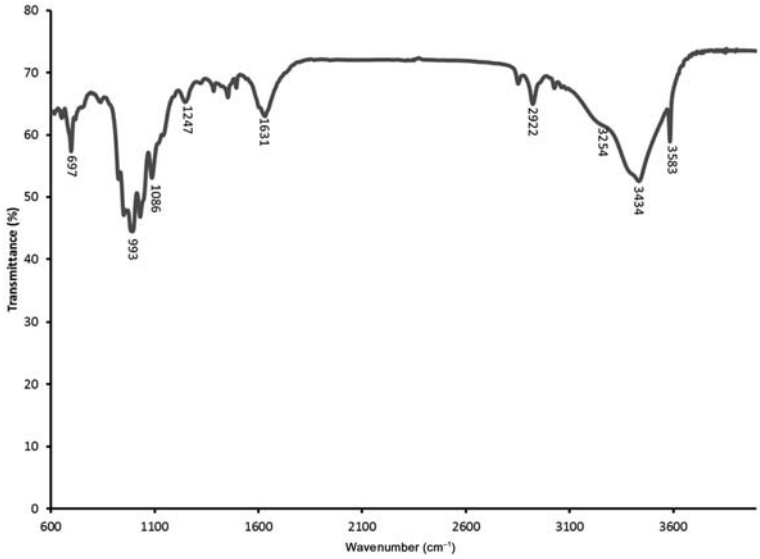

FIG. 4. FTIR spectrum of nolzeite.

applied and identical data merged to give 1361 reflections covering the entire Ewald sphere. Information pertaining to the data collection is given in Table 5.

Solution and refinement of the crystal structure of nolzeite were done using *SHELXL – 2014* (Sheldrick, 2008). The crystal structure was solved by direct methods, using the scattering curves of Cromer and Mann (1968) and the scattering factors of Cromer and Liberman (1970). Phasing of a set of normalized structure factors gave the mean $|E^2 - 1|$ value of 0.996, consistent with a centrosymmetric space group. In light of this and the absence of systematic extinctions, space group $P\bar{1}$. was chosen for the structure solution and refinement. Phase-normalized structure factors were used to give a difference-Fourier map from which one *Na*, three *Si*, two *Mn*, and several *O* sites were located. From subsequent difference-Fourier maps, a [4]-site with bond distances ranging from 1.317 to 1.608 Å was located. This site was assigned to B based on several arguments: (1) the mineral is morphologically, chemically, and on a crystal-structure basis, very similar to steedeite, $NaMn_2Si_3BO_9$(OH, a confirmed Na-Mn-borosilicate; (2) the two minerals occur together in the same samples from the same occurrence at Mont Saint-Hilaire, suggesting they arose via similar physio-chemical processes, including similar late-stage fluids; (3) refinement of the crystal structure indicates the presence of three [4]-sites attributable to Si and a fourth [4]-site, where bond distances are shorter-than-ideal for Si–O, but consistent with those for B–O and (4) qualitative EDS scans of both nolzeite and a member of the tourmaline supergroup (preliminary semi-quantitative EDS analyses indicate it to be the species, dravite) confirms the presence of B in both minerals. Determination of which *O* sites

TABLE 3. FTIR peaks and peak assignments for nolzeite.

Peak position (cm^{-1})	Assignment
3583	O–H stretching
3434	O–H stretching
3254	O–H stretching
2922	O–H stretching
2852	O–H stretching
1631	H–O–H bending
1247	B–OH bonds
1086	Asymmetric Si–O_{nbr}/B–O stretching
1030	Asymmetric Si–O_{nbr}/B–O stretching
993	Asymmetric Si–O_{nbr}/B–O stretching
951	Asymmetric Si–O_{nbr}/B–O stretching
925	Asymmetric Si–O_{nbr}/B–O stretching
839	Symmetric Si–O_{br} stretching
810	Symmetric Si–O_{br} stretching
697	Si–O–Si bending
652	Si–O–Si bending

TABLE 4. Powder X-ray diffraction data for nolzeite.

I_{obs}	I_{calc}	d_{meas} (Å)	d_{calc} (Å)	h	k	l
100	**100**	**10.113**	**10.131**	**0**	**0**	**$\bar{1}$**
16	**14**	**6.911**	**6.923**	**0**	**$\bar{1}$**	**0**
4	1	5.034	5.066	0	0	$\bar{2}$
13	**11**	**3.593**	**3.596**	**0**	**$\bar{1}$**	**3**
		3.520	3.522	0	$\bar{1}$	$\bar{2}$
	1		3.517	0	$\bar{2}$	2
	2		3.514	1	$\bar{2}$	0
	13	**3.026**	**3.032**	**0**	**$\bar{2}$**	**3**
		2.953	2.954	1	2	$\bar{1}$
50	**20**	**2.808**	**2.820**	**2**	**1**	**$\bar{1}$**
	21		**2.820**	**2**	**$\bar{2}$**	**0**
	1		**2.797**	**1**	**$\bar{1}$**	**$\bar{3}$**
	1		**2.787**	**1**	**$\bar{2}$**	**3**
7	4	2.767	2.778	2	1	$\bar{2}$
			2.777	2	$\bar{2}$	1
6	5	2.719	2.720	0	$\bar{1}$	4
12	**8**	**2.675**	**2.675**	**0**	**$\bar{1}$**	**$\bar{3}$**
12	4	2.463	2.469	0	$\bar{2}$	$\bar{2}$
	4		2.467	0	$\bar{3}$	2
4	2	2.284	2.292	2	0	$\bar{4}$
	2		2.290	2	$\bar{1}$	3
7	2	2.243	2.250	2	2	$\bar{2}$
			2.250	2	$\bar{3}$	1
6	2	2.173	2.180	2	2	$\bar{3}$
	2		2.180	2	$\bar{3}$	2
8	5	2.138	2.140	0	$\bar{1}$	$\bar{4}$
3	1	2.093	2.100	2	$\bar{1}$	$\bar{4}$
	1		2.099	2	0	3
3	1	2.068	2.069	0	$\bar{2}$	$\bar{3}$
7	1	2.024	2.029	2	2	$\bar{4}$
	1		2.029	2	$\bar{3}$	3
	2		2.026	0	0	$\bar{5}$
6	2	1.950	1.949	2	0	$\bar{5}$
	2		1.948	2	$\bar{1}$	4
4	1	1.897	1.906	0	$\bar{3}$	5
	1		1.906	2	$\bar{3}$	$\bar{2}$
	1		1.903	1	$\bar{4}$	2
2	1	1.838	1.836	0	$\bar{4}$	3
7	1	1.713	1.715	2	1	$\bar{6}$
	1		1.715	2	$\bar{2}$	5
	2		1.714	2	$\bar{3}$	$\bar{3}$
	1		1.714	2	2	2
5	2	1.687	1.689	0	0	$\bar{6}$
4	1	1.663	1.666	2	$\bar{4}$	$\bar{1}$
	1		1.666	2	3	0
3	1	1.630	1.637	2	3	$\bar{5}$
	1		1.637	2	$\bar{4}$	4
9	2	1.545	1.550	2	$\bar{4}$	$\bar{2}$
	2		1.550	2	3	1
	1		1.548	4	$\bar{2}$	$\bar{3}$
	1		1.548	4	0	1
4	2	1.498	1.506	2	1	$\bar{7}$
	2		1.505	2	$\bar{2}$	6
5	1	1.481	1.481	0	$\bar{4}$	$\bar{2}$
3	1	1.445	1.449	4	$\bar{2}$	$\bar{4}$
	1		1.449	4	0	2
	1		1.447	0	0	$\bar{7}$
5	2	1.405	1.407	0	$\bar{5}$	5
5	1	1.331	1.334	2	1	$\bar{8}$
	1		1.334	2	$\bar{2}$	7
4	1	1.306	1.309	0	$\bar{5}$	$\bar{1}$

(continued on next column)

TABLE 4. (*contd.*)

Strongest lines are given in bold.

were occupied by OH or H_2O was based on bond-valence calculations and electroneutrality considerations (Table 6).

Refinement of this model converged to R = 12.81% and wR^2 = 29.80%. The relatively high R-factor for the refined crystal structure of nolzeite is attributed to the fact that the crystal studied by single-crystal X-ray diffraction (SXRD) was extremely thin in two directions (measuring 7 μm × 8 μm × 60 μm) and that it may not have been

TABLE 5. Miscellaneous single-crystal data for nolzeite.

a (Å)	6.894(1)
b	7.632(2)
c	11.017(2)
α (°)	108.39(3)
β	99.03(3)
γ	103.05(3)
V (Å^3)	519.27(1)
Space group	$P\bar{1}$ (#2)
Z	2
D_{calc} (g/cm^{-3})	2.79
Crystal size (μm)	7 × 8 × 60
Radiation	Mo$K\alpha$ (50 kV, 40 mA)
Monochromator	Graphite
Intensity-data collection	θ:2θ
Criterion for observed reflections	$F_o > 4\sigma(F_o)$
Goof	2.000
Total No. of reflections collected	9610
No. unique reflections	1361
No. observed reflections	918
R (int %)	4.75
R (sym %)	7.13
R %	12.81
wR^2 %	29.80

TABLE 6. Bond-valence table (vu) for nolzeite*.

	Na	Mn(1)	Mn(2)	Si(1)	Si(2)	Si(3)	B	Σ
O1		$0.577^{\downarrow\rightarrow}$	$0.281^{\downarrow\rightarrow}$			$1.027^{\downarrow\rightarrow}$		1.885
O2		$0.246^{\downarrow\rightarrow}$	$0.565^{\downarrow\rightarrow}$		$1.022^{\downarrow\rightarrow}$			1.833
O3	$0.273^{\downarrow\rightarrow}$	$0.308^{\downarrow\rightarrow}$	$0.313^{\downarrow\rightarrow}$	$0.898^{\downarrow\rightarrow}$				1.792
O4						$1.050^{\downarrow\rightarrow}$	$0.706^{\downarrow\rightarrow}$	1.756
O5		$0.347^{\downarrow\rightarrow}$	$0.348^{\downarrow\rightarrow}$	$1.061^{\downarrow\rightarrow}$				1.756
O6	$0.138^{\downarrow\rightarrow}$			$0.793^{\downarrow\rightarrow}$	$1.027^{\downarrow\rightarrow}$			1.958
O7					$1.093^{\downarrow\rightarrow}$		$0.692^{\downarrow\rightarrow}$	1.785
O8	$0.094^{\downarrow\rightarrow}$			$0.819^{\downarrow\rightarrow}$		$0.989^{\downarrow\rightarrow}$		1.902
O9	$0.156^{\downarrow\rightarrow}$				$0.869^{\downarrow\rightarrow}$	$0.905^{\downarrow\rightarrow}$		1.93
OH10							$0.968^{\downarrow\rightarrow}$	0.968
OH11	$0.104^{\downarrow\rightarrow}$		$0.254^{\downarrow\rightarrow}$				$0.576^{\downarrow\rightarrow}$	0.934
OW12	$0.302^{\downarrow\rightarrow}$							0.302
OW13	$0.186^{\downarrow\rightarrow}$	$0.273^{\downarrow\rightarrow}$						0.459
Σ	1.253	1.751	1.761	3.571	4.011	3.971	2.942	

*Bond valences for other sites determined using parameters from Brese and O'Keeffe (1991).

truly single. Although preliminary examination of this crystal with a polarized-light microscope indicated a sharp, strong extinction, implying it was single, further examination of the SXRD data revealed a subtle, but detectable, splitting of some diffraction spots, suggesting that the crystal may not in fact have been truly single. Single-crystal data produced from this crystal gave $R_{int} = 4.75\%$ and $R_{sym} = 7.13\%$. In light of this, a second SXRD data collection was attempted on an even thinner crystal measuring 4 μm × 6 μm × 50 μm, the data from which did not indicate any pronounced splitting of diffraction spots, i.e. that it was single. However, the second crystal was found to be an extremely poor X-ray scatterer (presumably due to its fine acicular size), i.e. significantly less than that for the first crystal, for which data were produced out to $2\theta = 60°$. Despite the reduction in observable data for the second crystal, attempts were made to refine the crystal structure but these were unsuccessful, as the *R*-factor could not be reduced below 30%.

Crystal structure

Cation polyhedra

The crystal structure of nolzeite contains three *Si* sites, two *Mn* sites, and two unique *Na* and *B* sites (Table 7). All of the sites were found to be fully occupied with the exception of the *Mn* sites which refined to site occupancies of 0.85. The three *Si* sites are coordinated by four crystallographically distinct O atoms with Si–O bond lengths ranging from 1.60(1) to 1.69(1) Å (Table 8). The *B* site is coordinated by two O atoms and two (OH) groups, forming a $BO_2(OH)_2$ tetrahedron with B–(O,OH) bond lengths ranging from 1.32(4) to 1.61(3) Å (Table 7). This type of B–O tetrahedron is extremely unusual, having only been reported in two other minerals: rogermitchellite [$Na_{12}(Sr,Na)_{24}Ba_4Zr_{26}Si_{78}(B,Si)_{12}O_{246}(OH)_{24}\cdot 18H_2O$; McDonald and Chao, 2010] and steedeite [$NaMn_2Si_3BO_9(OH)_2$; Haring and McDonald, 2014], both of which are known to occur only at Mont Saint-Hilaire. The site attributed to B has B–(O,OH) lengths ranging from 1.32(4) to 1.61(3) Å with an average <B–O> length of 1.52 Å. The range of B–(O,OH) lengths in nolzeite is greater than those observed in rogermitchellite (1.49–1.52 Å) (McDonald and Chao, 2010) and steedeite (1.468–1.508 Å) (Haring and McDonald, 2014). For these three minerals, there appears to be no correlation between B–(O,OH) bond length and whether or not B is bonded to O or an OH group. Instead the range of B–(O,OH) lengths observed in nolzeite may be attributed to Si↔B substitution on the *B* site (see discussion below). The average <B–(O,OH)> length in nolzeite is slightly longer than the ideal length of 1.477 Å for B in tetrahedral coordination (Hawthorne *et al.*, 1996). We attribute this longer-than-ideal bond distance to significant (~30%) B ↔ Si substitution in the site (Fig. 5), a fact supported by SEM-EDS data for the mineral which show an excess in SiO_2 over that predicted for an ideal amount (i.e. 44.17 *vs*. 40.78 wt.% SiO_2). The ~30% substitution of B with Si is

TABLE 7. Atomic coordinates (Å^2) and displacement parameters for nolzeite.

Atom	*x*	*y*	*z*	s.o.f.	U^{11}	U^{22}	U^{33}	U^{23}	U^{13}	U^{12}	U_{eq}
Na1	0.821(1)	0.072(1)	–0.239(1)	1	0.044(6)	0.057(6)	0.057(7)	0.012(5)	0.010(5)	0.020(5)	0.054(3)
Mn1	0.9536(4)	–0.2913(4)	–0.4112(3)	0.85	0	0.012(2)	0.015(2)	0.004(1)	0.004(1)	0.005(1)	0.009(1)
Mn2	0.5558(4)	–0.7001(4)	–0.5925(3)	0.85	0	0.011(2)	0.015(2)	0.005(1)	0.004(1)	0.004(1)	0.009(1)
Si1	1.3001(9)	0.1011(9)	–0.4088(6)	1	0.013(3)	0.037(4)	0.036(4)	0.007(3)	0.009(3)	0.010(3)	0.030(2)
Si2	1.6857(8)	–0.5657(8)	–0.2701(5)	1	0.015(3)	0.022(3)	0.025(3)	0.009(3)	0.005(3)	0.010(3)	0.020(1)
Si3	1.1474(8)	–0.5689(8)	–0.2708(5)	1	0.012(3)	0.019(3)	0.029(3)	0.010(3)	0.008(3)	0.006(2)	0.019(1)
B	1.529(3)	–0.285(4)	–0.087(4)	0.7	0.051(2)	0.10(2)	0.25(4)	0.10(3)	0.05(2)	0.04(1)	0.12(1)
Si				0.3							
O1	1.155(2)	–0.483(2)	–0.388(1)	1	0.004(7)	0.022(7)	0.026(8)	–0.007(6)	–0.003(6)	0.006(6)	0.018(3)
O2	1.661(2)	–0.485(2)	–0.389(1)	1	0.013(7)	0.024(7)	0.024(7)	0.012(6)	0.010(6)	0.006(6)	0.018(3)
O3	1.281(2)	0.144(2)	–0.548(1)	1	0.011(7)	0.031(8)	0.038(9)	0.013(7)	0.010(6)	0.012(7)	0.025(3)
O4	1.311(2)	–0.429(2)	–0.133(1)	1	0.005(7)	0.07(1)	0.025(8)	0.013(8)	0.005(6)	0.013(7)	0.035(4)
O5	1.242(2)	–0.123(2)	–0.425(1)	1	0.006(7)	0.032(8)	0.041(9)	0.019(7)	0.010(6)	0.010(6)	0.024(3)
O6	1.544(2)	–0.787(2)	–0.315(1)	1	0.024(8)	0.024(8)	0.037(9)	0.006(7)	0.001(7)	0.004(7)	0.031(4)
O7	1.667(2)	–0.426(2)	–0.133(1)	1	0.027(9)	0.039(9)	0.029(9)	0	0.007(7)	0.012(7)	0.034(4)
O8	1.155(2)	–0.791(2)	–0.317(1)	1	0.029(9)	0.04(1)	0.05(1)	0.009(7)	0.018(7)	0.009(7)	0.038(5)
O9	0.921(2)	–0.587(2)	–0.231(1)	1	0	0.06(1)	0.05(1)	0.015(8)	0.014(7)	0.016(7)	0.036(4)
OH10	1.585(2)	–0.186(2)	0.041(1)	1	0.015(8)	0.05(1)	0.012(7)	–0.004(7)	–0.002(6)	0.016(7)	0.030(4)
OH11	1.542(2)	–0.162(2)	–0.180(1)	1	0.020(8)	0.05(1)	0.031(8)	0.012(7)	0.007(7)	0.024(7)	0.033(4)
OW12	0.926(2)	0.230(2)	–0.018(1)	1	0.018(8)	0.06(1)	0.032(8)	0.022(8)	0.018(7)	0.023(7)	0.030(4)
OW13	1.046(2)	–0.113(2)	–0.191(1)	1	0.024(9)	0.06(1)	0.031(9)	0.001(8)	0.005(7)	0.021(8)	0.040(4)

s.o.f. – site occupancy factor.

TABLE 8. Interatomic distances (Å) in nolzeite.

NaO_4(OH)(H_2O)$_2$ Polyhedron			*Si*(1)O_4 Tetrahedron		
Na	–OW12	2.26(2)	*Si*1	–O5	1.61(1)
	–O3	2.28(2)		–O3	1.66(1)
	–OW13	2.42(2)		–O8	1.69(1)
	–O9	2.50(2)		–O6	1.69(1)
	–O6	2.55(2)	<*Si*1–O>		1.66
	–OH11	2.63(2)			
	–O8	2.69(2)	*Si*(2)O_4 Tetrahedron		
<*Na*–O>		2.48	*Si*2	–O7	1.60(1)
				–O2	1.62(1)
Mn(1)O_5(H_2O) Octahedron				–O6	1.62(1)
*Mn*1	–O5	2.16(1)		–O9	1.67(1)
	–O1	2.22(1)	<*Si*2–O>		1.63
	–O3	2.23(1)			
	–O1	2.27(1)	*Si*(3)O_4 Tetrahedron		
	–OW13	2.27(1)	*Si*3	–O4	1.62(1)
	–O2	2.31(1)		–O8	1.62(1)
<*Mn*1–O>		2.24		–O1	1.62 (1)
				–O9	1.67(1)
Mn(2)O_5(OH) Octahedron			<*Si*3–O>		1.63
*Mn*2	–O5	2.17(1)			
	–O3	2.21(1)	*B*O_2(OH)$_2$ Tetrahedron		
	–O2	2.21(1)	*B*	–OH10	1.32(4)
	–O1	2.25(1)		–O4	1.55(3)
	–O2	2.30(1)		–OH11	1.59(3)
	–OH11	2.31(1)		–O7	1.61(3)
<*Mn*2–O>		2.24	<*B*–O>		1.52

estimated based on chemical data as well as the unusually long B–O bond lengths.

The two *Mn* sites are octahedrally coordinated with a combination of O anions as well as OH and H_2O groups. Two distinct types of $MnO_5\varphi$ (φ = OH, H_2O) octahedra occur in the crystal structure of nolzeite: (1) Mn(1)O_5(H_2O) octahedra and (2) Mn(2)O_5(OH) octahedra. Both have similar Mn–(O,OH,H_2O) bond lengths, ranging from 2.16(1) to 2.31(1) Å (Table 8), which are consistent with the Mn–(O,OH) bonds observed in sérandite (Jacobsen *et al*., 2000). The *Na* site is coordinated by four O atoms, one (OH) group, and two (H_2O) groups, forming *Na*O_4(OH)(H_2O)$_2$ polyhedra, with Na–(O, OH,H_2O) bond lengths ranging from 2.26(2) to 2.69 (2) Å (<Na-(O,OH)> = 2.48 Å, Table 5).

Bond topology

Each SiO_4 tetrahedron in the crystal structure of nolzeite is linked to two adjacent SiO_4 tetrahedra through shared corners, forming infinite single silicate chains parallel to *a* (i.e. the elongation direction). The silicate chains have a repeat unit consisting of three symmetrically independent SiO_4 tetrahedra: Si(1)O_4, Si(2)O_4 and Si(3)O_4, forming *C*-shaped clusters (Fig. 6). These clusters are closed by $BO_2(OH)_2$ tetrahedra *via* shared corners, generating four-membered $[BSi_3O_{12}]^{7-}$ rings (Fig. 6). The $BO_2(OH)_2$ tetrahedra are therefore branching tetahedra so the silicate chain in nolzeite can be classed as a loop-branched *dreier* chain silicate (Liebau, 1978). Such borosilicate chains are unusual and have been found in only one other naturally occurring mineral, steedeite (Haring and McDonald, 2014). The loop-branched tetrahedral chains are linked through shared corners to double

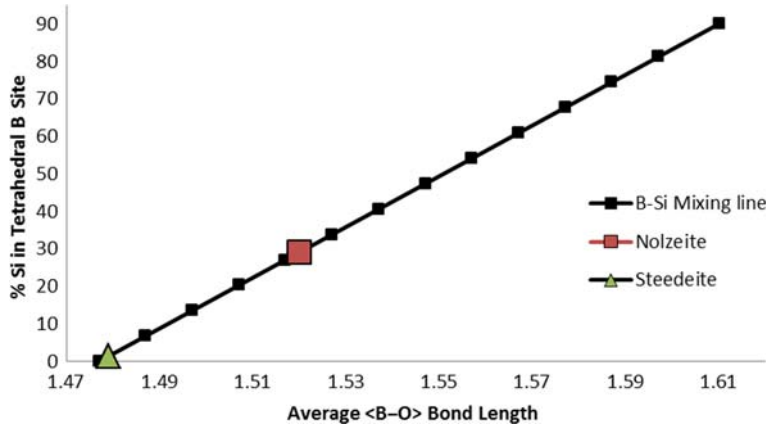

FIG. 5. The relation between average <B–O> bond length and the proportion (%) of Si atoms within the B site. The %Si was obtained using the following formula: %Si = [(observed <B–O> – 1.477)/(1.630–1.477] * 100.

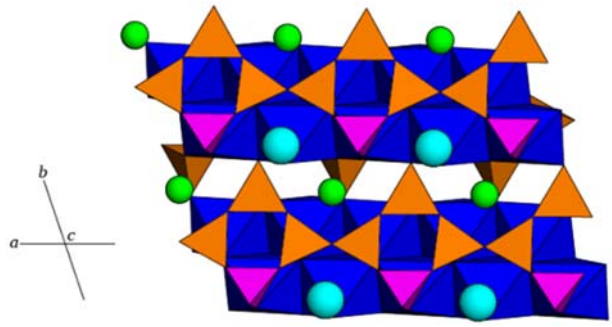

FIG. 6. crystal structure of nolzeite projected on to [011]. Both the bands of $MnO_5(OH)$ and the loop-branched *dreier* chains run parallel to *a*. Dark blue octahedra = $MnO_5(OH)$, orange tetrahedra = SiO_4, pink tetrahedra = $BO_2(OH)_2$, light blue spheres = H_2O and green spheres = Na.

chains of edge-sharing $MnO_5\varphi$ octahedra completing the 3D structure. The loop-branched silicate chains and $MnO_5(OH)$ chains form distinct tetrahedral (*T*) and octahedral (*O*) layers, respectively, resulting in a *T–O–T–O*… stacking sequence perpendicular to {101} (Fig. 7). This stacking orientation is slightly different from that of steedeite, where the T–O stacking is perpendicular to {011}, resulting in the variation in refractive indices and Raman spectra between the two minerals. The stacking pattern in nolzeite, along with the linkages between the layers of tetrahedra and octahedra, gives rise to an *I*-beam topology (Thompson, 1970). These 'I-beams' are linked through shared corners to adjacent ones to form layers along {001}, which alternate with layers containing the $NaO_4(OH)(H_2O)_2$ polyhedra.

Related structures

The *I*-beam topology and the *T–O–T* stacking pattern present in nolzeite is similar to that found in other chain silicate minerals, specifically steedeite, as well as pyroxenoids of the pectolite ($NaCa_2[Si_3O_8OH]$)–sérandite ($NaMn_2[Si_3O_8OH]$) series, which are also hydrated and have *P* symmetry.

The crystal structure of nolzeite most closely resembles that of steedeite as the single loop-branched

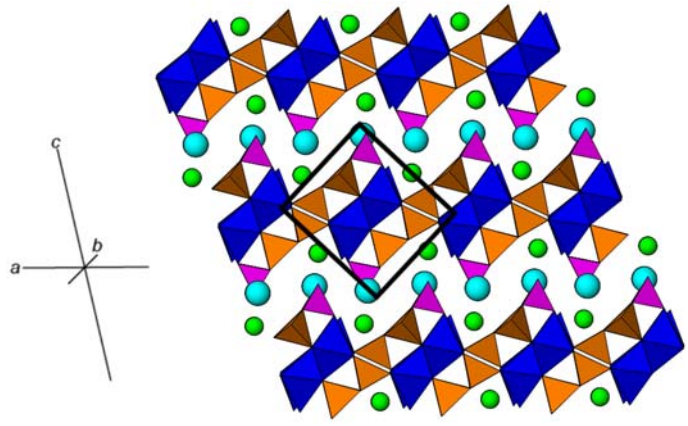

FIG. 7. The crystal structure of nolzeite with layers of tetrahedra and octahedra alternating along [011] generating an *I*-beam topology. The Mn-borosilicate *I*-beams (outlined in black) form distinct layers that alternate with layers containing water and sodium along [001]. Dark blue octahedra = $MnO_5(OH)$, orange tetrahedra = SiO_4, pink tetrahedra = $BO_2(OH)_2$, light blue spheres = H_2O, green spheres = Na.

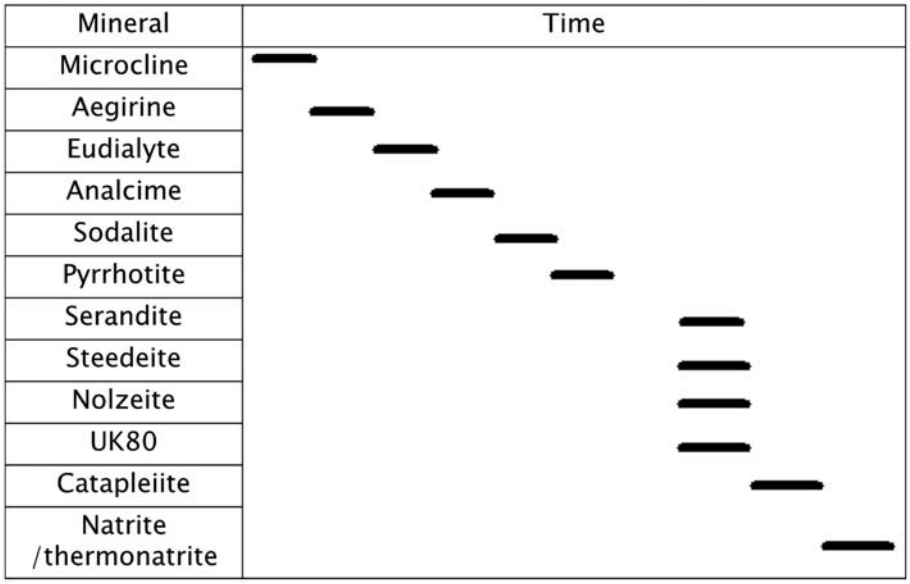

FIG. 8. Paragenetic sequence for nolzeite and other minerals in vugs in a single xenolith at Mont Saint-Hilaire, Québec, Canada.

dreier borosilicate chains present are identical to those in steedeite (Haring and McDonald, 2014). The crystal structures of pectolite–sérandite series pyroxenoids also consist of *dreier* silicate chains (Waldemar, 1955; Prewitt, 1967) similar to those in nolzeite, but differ in that they are unbranched *dreier* chains (Fig. 4). Nolzeite, steedeite and members of the pectolite–sérandite series also all contain double chains of edge-sharing octahedra. Chemically, nolzeite has proportions of Na, Mn and Si identical to those of steedeite, but nolzeite contains H_2O groups and has a mixed B/Si site.

The crystal structure of nolzeite is also similar to that of scheuchzerite $\{Na(Mn,Mg)_9[VSi_9O_{28}(OH)](OH)_3\}$; Brugger *et al*., 2006). Both minerals have hydrated loop-branched chain silicate structures but the silicate chains in scheuchzerite are more complex, with a periodicity of seven and six-membered silicate rings that alternate with *C*-shaped silicate clusters (Brugger *et al.,* 2006; Fig. 4). Each six-membered silicate ring within the silicate chain in scheuchzerite is linked through a shared corner to a single tetrahedron $(VO_4)^{3-}$ tetrahedron (Brugger *et al*., 2006). The $(VO_4)^{3-}$ group is considered to be a branching tetrahedron, therefore the silicate chain in scheuchzerite can be considered as being both loop-branched and open branched (Liebau, 1978). The crystal structures of scheuchzerite and nolzeite both contain bands of edge-sharing $Mn(O,OH)_6$ octahedra. The bands of $Mn(O,OH)_6$ octahedra in scheuchzerite (Brugger *et al*., 2006) are wider than those in nolzeite, with a single band of octahedra varying from three to four octahedra wide, while that in nolzeite is only two octahedra wide.

There are also two synthetic phases, $Li_2Mg_2(Si_4O_{11})$ (Maresch and Czank, 1985; Czank and Bissert, 1993) and $Fe_3Be(Si_3O_9)(F,OH)_2$ (Bakakin and Solov'eva, 1971) that have single loop-branched *dreier* chains similar to those in nolzeite. The crystal structure of $Li_2Mg_2(Si_4O_{11})$, as in nolzeite, has tetrahedral chains consisting of *C*-shaped clusters of three SiO_4 tetrahedra. These clusters are closed by a fourth SiO_4 tetrahedron [rather than a $BO_2(OH)_2$ tetrahedron as in nolzeite] generating four-membered $(Si_4O_{11})^{6-}$ rings (Czank and Bissert, 1993; Fig. 4). The silicate chains are linked through shared corners to double chains or bands of edge-sharing MgO_6 octahedra (Czank and Bissert, 1993). The crystal structure of $Fe_3Be(Si_3O_9)(F,OH)_2$ contains loop-branched *dreier* silicate chains similar to those in nolzeite but with BeO_4 tetrahedra instead of $BO_2(OH)_2$ tetrahedra closing the *C*-shaped silicate clusters. The silicate chains in $Fe_3Be(Si_3O_9)(F,OH)_2$ are linked through shared corners to triple chains of edge-sharing FeO_6 octahedra.

Origin

Paragenetically, nolzeite, along with sérandite, steedeite, UK80, and thermonatrite are late-stage phases which overgrow earlier-formed phases such as microcline, aegirine and analcime (Fig. 8). Thermonatrite is inferred to have been the latest crystallizing phase. The paragenetic sequence of nolzeite relative to sérandite, steedeite and UK80 is unclear (Fig. 8), as none have been found together in the same vug (see discussion below).

In general, the hydrous structure of nolzeite and its occurrence in vugs suggests that it crystallized from late-stage aqueous fluids. These fluids are inferred to have been highly alkaline due to the presence of late-stage natrite (Fig. 8). Experimental studies showed that the maximum stability of the latter mineral is in the pH range of ~ 8 to 10 (Marion, 2001). On the basis of fluid-inclusion data as well as carbonate-carbonate and carbonate-silicate equilibria, the temperatures of late-stage fluids at Mont Saint-Hilaire are inferred to have been <400°C (Schilling *et al*., 2011). The occurrence of nolzeite, steedeite, sérandite and the unidentified mineral UK80 in vugs of the same xenolith, suggests that these minerals precipitated from similar late-stage aqueous fluids. The presence of late-stage sérandite (Fig. 8) in the same sample as nolzeite and steedeite also suggests that the aqueous fluid had localized variations in $a_{[SiO_2]^{4-}}$ as well as $a_{B(OH)_3}$ and $a_{[B(OH)_4]^-}$, whereas a decrease in $a_{[SiO_2]^{4-}}$ and an increase in both $a_{B(OH)_3}$ and $a_{[B(OH)_4]^-}$ favoured the development of nolzeite and steedeite over sérandite (Haring and McDonald, 2014). Due to the possible variations in $a_{B(OH)_3}$ in the late-stage fluids, it is unclear whether or not the crystal structure of UK80 also contains B.

Another indication for the low-*T* formation of nolzeite may be the conditions at which minerals of the sérandite–pectolite series form (Haring and McDonald, 2014; Clark and Bunn 1940; Blakeman *et al*., 1974; Xi and Glasser, 1984). Given the existence of late-stage sérandite in the same boulder wherein nolzeite was found implies that nolzeite probably formed under a similar range in *T*. It is noteworthy that nolzeite and steedeite are the only minerals known to contain single looped-branched *dreier* silicate chains, suggesting that they may be stable over a very narrow *P*–*T* range (Haring and McDonald, 2014).

Acknowledgements

The authors thank Dr. F.C. Hawthorne (Dept. of Geological Sciences, University of Manitoba) for providing access to the three-circle diffractometer and to Mr. Mark. A. Cooper for assistance with the single-crystal XRD data collection. In addition Dr. Joy Gray-Munro (Department of Chemistry and Biochemistry, Laurentian University) is thanked for providing access to the infrared spectrometer as well as assistance with the data collection. The authors also acknowledge the comments made by the structures editor, Dr. Peter Leverett and the referees, Dr. Edward S. Grew and Dr. Joel Grice as well as an anonymous referee. Financial support to MMMH was provided through an Alexander Graham Bell Canada Graduate Scholarship, provided by the Natural Sciences and Engineering Research Council.

References

Bakakin, V.V. and Solo'eva, L.P. (1971) Crystal structure of $Fe_3BeSi_3O_9(F,OH)_2$, an example of a wollastonite-like silicon-oxygen chain based on Fe. *Soviet Physics Crystallography*, **15**, 999–1005.

Blakeman, E.A., Gard, J.A., Ramsay, C.G. and Taylor, H. F.W. (1974) Studies on the system sodium oxide – calcium oxide – silica – water. *Journal of Chemical Technology and Biotechnology*, **24**, 239–245.

Brese, N.E. and O'Keeffe, M. (1991) Bond-valence parameters for solids. *Acta Crystallographica*, **B47**, 192–197.

Brugger, J., Krivovichev, S., Meisser, N., Ansermet, S. and Armbruster, T. (2006) Scheuchzerite, Na(Mn, $Mg)_9[VSi_9O_{28}(OH)](OH)_3$, a new single-chain silicate. *American Mineralogist*, **91**, 937–943.

Chao, G.Y., Conlon, R.P. and Velthuizen, J. (1990) Mont Saint-Hilaire Unknowns. *The Mineralogical Record*, **21**, 363–368.

Clark, L.M. and Bunn, C.W. (1940) The scaling of boilers. Pt. IV. Identification of phases in calcium silicate scales. *Journal of the Society of Chemical Industry*, **59**, 155–158.

Cromer, D.T. and Liberman, D. (1970) Relativistic calculation of anomalous scattering factors for X rays. *Journal of Physical Chemistry*, **53**, 1891–1898.

Cromer, D.T. and Mann, J.B. (1968) X-ray scattering factors computed from numerical Hartree-Frock wave functions. *Acta Crystallographica*, **A24**, 321–324.

Czank, M. and Bissert, G. (1993) The crystal structure of $Li_2Mg_2[Si_4O_{11}]$, a loop-branched dreier single chain silicate. *Zeitschrift für Kristallographie*, **204**, 129–142.

Dowty, E. (2009) *VIBRATZ for Windows and Macintosh Version 2.2*. Shape Software, Kingsport, Tennessee, USA.

Frisch, M.J., Trucks, G.W. Schlegel, H.B., *et al*. (2013) *Gaussian 09, Revision D.01*. Gaussian, Inc., Wallingford, Connecticut, USA.

Frost, R.L., Bouzaid, J.M., Martens, W.N. and Reddy, J.B. (2007) Raman spectroscopy of the borosilicate mineral

ferroaxinite. *Journal of Raman Spectroscopy*, **38**, 135–141.

Haring, M.M.M. and McDonald, A.M. (2014) Steedeite, $NaMn_2[Si_3BO_9](OH)_2$: Characterization, crystal-structure determination, and origin. *The Canadian Mineralogist*, **52**, 47–60.

Hawthorne, F.C., Burns, P.C. and Grice, J.D. (1996) The crystal chemistry of boron. Pp. 41–110 in: *Boron: Mineralogy, Petrology, and Geochemistry* (L.M. Anovitz and E.S. Grew, editors) Reviews in Mineralogy, **33**. Mineralogical Society of America, Washington DC.

Jacobsen, S.D., Smyth, J.R., Swope, J.R., and Sheldon, R. I. (2000) Two proton positions in the very strong hydrogen bond of sérandite, $NaMn_2[Si_3O_8(OH)]$. *American Mineralogist*, **85**, 745–752.

Kraus, W. and Nolze, G. (1996) Powder Cell – a program for the representation and manipulation of crystal structures and calculation of the resulting x-ray powder patterns. *Journal of Applied Crystallography*, **29**, 301–303.

Liebau, F. (1978) Silicates with branched anions: a crystallochemically distinct class. *American Mineralogist*, **63**, 918–923.

Mandarino J.A. (1981) The Gladstone–Dale relationship. IV. The compatibility concept and its application. *The Canadian Mineralogist*, **19**, 441–450.

Maresch, W.V. and Czank, M. (1985) The optical and X-ray properties of $Li_2Mg_2[Si_4O_{11}]$, a new type of chain-silicate. *Neues Jahrbuch für Mineralogie*, **7**, 289–297.

Marion, G.M. (2001) Carbonate mineral solubility at low temperatures in the Na-K-Mg-Ca-H-Cl-SO_4-OH-HCO_3-CO_3-CO_2-H_2O system. *Geochimica et Cosmochimica Acta*, **65**, 1883–1896.

McDonald, A.M. and Chao, G.Y.(y2005)| Bobtraillite, $(Na,Ca)_{13}Sr_{11}(Zr,Y,Nb)_{14}Si_{42}B_6O_{132}(OH)_{12}\cdot 12H_2O$ a new mineral species from Mont Saint-Hilaire, Québec: description, structure determination and relationship to benitoite and wadeite. *The Canadian Mineralogist*, **43,** 747–758.

McDonald, A.M. and Chao, G.Y. (2010) Rogermitchellite, $Na_{12}(Sr,Na)_{24}Ba_4Zr_{26}Si_{78}(B,Si)_{12}O_{246}(OH)_{24}\cdot 18H_2O$, a new mineral species from Mont Saint-Hilaire, Québec: description, structure determination and relationship with HFSE-bearing cyclosilicates. *The Canadian Mineralogist*, **48**, 267–278.

Nolze, G., Geist, V., Neumann, R.S. and Buchheim, M. (2005) Investigation of orientation relationships by EBSD and EDS on the example of the Watson iron meteorite. *Crystallographic Research and Technology*, **40**, 791–804.

Prewitt, C.T. (1967) Refinement of the crystal structure of pectolite, $Ca_2NaHSi_3O_9$. *Zeitschrift für Kristallographie*, **125**, 298–316.

Schilling, J., Marks, M.A.W., Wenzel, T., Vennemann, T., Horvath, L., Tarassoff, P., Jacob, D.E., and Markl, G. (2011) Magmatic to hydrothermal evolution of the intrusive Mont Saint-Hilaire complex: insights into the late-stage evolution of peralkaline rocks. *Journal of Petrology*, **52**, 2147–2185.

Sheldrick, G.M. (2008) A short history of *SHELX*. *Acta Crystallographica*, **A64**, 112–122.

Thompson, J.B. (1970) Geometrical possibilities for amphibole structures: Model biopyriboles. *American Mineralogist*, **63**, 239–249.

Waldemar, T.S. (1955) The pectolite-serandite series. *American Mineralogist*, **40**, 1022–1031.

Williams, Q. (1995) Infrared, Raman and optical spectroscopy of Earth materials. Pp. 291–302 in: *Mineral Physics and Crystallography: A Handbook of Physical Constants*, (T.J. Ahrens, editor). American Geophysical Union, Washington, DC.

Xi, Y. and Glasser L.S.D. (1984) Hydrothermal study in the system Na2O-CaO-SiO2-H2O at 300 degrees celcius. *Cement Concrete Research*, **14**, 741–748.